Direct Detection of Down-Converted Photons Spontaneously Produced at a Single Josephson Junction

Dorian Fraudet,[1] Izak Snyman,[2] Denis M. Basko,[3] Sébastien Léger,[1,4] Théo Sépulcre,[5] Arpit Ranadive,[1] Gwenael Le Gal,[1] Alba Torras-Coloma,[6,7] Wiebke Guichard,[1] Serge Florens,[1] and Nicolas Roch[1]

[1]*Université Grenoble Alpes, CNRS, Grenoble INP, Institut Néel, 38000 Grenoble, France*
[2]*Mandelstam Institute for Theoretical Physics, School of Physics, University of the Witwatersrand, Johannesburg, South Africa*
[3]*Université Grenoble Alpes, CNRS, LPMMC, 38000 Grenoble, France*
[4]*Department of Physics and Applied Physics, Stanford University, Stanford, California 94305, USA*
[5]*Wallenberg Centre for Quantum Technology, Chalmers University of Technology, SE-412 96 Gothenburg, Sweden*
[6]*Institut de Física d'Altes Energies (IFAE), The Barcelona Institute of Science and Technology (BIST), Bellaterra (Barcelona) 08193, Spain*
[7]*Departament de Física, Universitat Autònoma de Barcelona, 08193 Bellaterra, Spain*

(Received 1 May 2024; revised 5 September 2024; accepted 1 November 2024; published 9 January 2025)

We study spontaneous photon decay into multiple photons triggered by strong nonlinearities in an experimental simulator of a bosonic quantum impurity model. Previously, spectroscopic signatures of photon conversion were reported and evidenced as resonances in the many-body spectrum of these systems. Here, we report on the observation of multimode fluorescence of a small Josephson junction embedded in a high impedance superconducting transmission line. Measurement of the down-converted photons is achieved using state-of-the-art broadband parametric amplifiers. Photon triplet emission is explicitly demonstrated at a given frequency as the counterpart of inelastic photon decay at 3× the emission frequency. These results open exciting prospects for the burgeoning field of many-body quantum optics and offer a direct signature of the ultrastrong light-matter coupling.

DOI: 10.1103/PhysRevLett.134.013804

Introduction—Circuit quantum electrodynamics (cQED) [1] constitutes an ideal playground for quantum simulation [2,3] due to the versatility in model Hamiltonian designs. Simulators of quantum impurities comprise a class of quantum many body systems that require low hardware overhead in cQED. They are well studied in traditional condensed matter, and can be obtained in cQED by coupling a large set of harmonic resonators to a single nonlinear element placed at the boundary of the circuit. Such simulators offer tunability both for the "speed of light" propagating through the harmonic modes, and for the single "atom" properties, that are hard to engineer in the quantum optics context. Reaching the true quantum many-body regime relies on two important pillars. First, the superstrong coupling regime [4], in which the impurity spectral width is larger than the free spectral range (the frequency spacing between two consecutive harmonic modes), is required to obtain broadband photon emission. This was recently reported in cQED using very long distributed microwave resonators [5] or slow light (high impedance) transmission lines made of Josephson junction (JJ) arrays [6,7]. Second, strong nonlinearity is required to open up the phase space of inelastic decay channels involving multiphoton states. This condition was demonstrated [8–12] for Josephson junctions designed with a small Josephson energy (E_J) to charging energy (E_c) ratio. Fully understanding experimental cQED quantum impurity simulators is a clear prerequisite before addressing the more challenging physics of bulk versions of the sine-Gordon model [13,14].

Many-body extensions of several cornerstones in quantum optics have been demonstrated in recent years using cQED impurity simulators. For instance, the tiny Lamb shift of quantum optics was shown to turn into a giant renormalization of the impurity frequency [8,9,11], an effect originating from the ultrastrong coupling to a dissipative bath [15,16]. In addition, extremely large inelastic photon losses were reported in Refs. [10,11], and interpreted from multiphoton down-conversion processes, following theoretical predictions [17–23]. More direct evidence for multiphoton conversion were the remarkable observations of avoided crossings between multiphoton states [12,24], which can be understood as a many-body version of the celebrated vacuum Rabi splitting [25]. However, those studies relied mainly on single-frequency spectroscopic measurements, and the direct evidence of photon down-conversion processes in quantum impurity simulators is still lacking.

In this Letter, we present the observation of down-converted photons produced in a quantum impurity system, highlighting the importance of frequency conversion for dissipative structures in open quantum systems [26] and showing a possibility to control this dissipation channel. Our setup can also serve as a source of entangled microwave photon triplets, potentially useful in quantum information domain, thus addressing a long-standing challenge in optics [27]. Complementary to the stimulated upconversion process observed by Vrajitoarea *et al.* [28], our demonstration verifies theoretical predictions [29,30] that spontaneous frequency conversion is possible in the ultrastrong coupling regime without the need for a strong classical pump. This contrasts sharply with experiments on driven quantum impurities [31] and with previous observations of frequency conversion relying on parametric processes [32–34] or cascaded photon emission [35], where very strong drives were required.

Experimental setup—In previous quantum impurity simulator experiments [9–11], it was extremely challenging to observe the down-converted photons because there were too many possible final states for the decay of a photon with frequency ω_{in} into several photons with frequencies ω_k fulfilling $\omega_{\mathrm{in}} = \Sigma_k \omega_k$. The output power at each mode ω_k was simply too low to be resolved within a reasonable integration time. To circumvent this problem, we designed here a shorter transmission line, leading to a larger free spectral range of the order of 3 GHz.

The device under study, depicted in Fig. 1, consists of a microwave multimode Fabry-Perot resonator represented by an array of $N = 200$ JJs. The array junctions are in the linear regime ($E_{\mathrm{J}}^{\mathrm{arr}}/E_{\mathrm{c}}^{\mathrm{arr}} \sim 300$) and act as high inductances $L = (\hbar/2e)^2/E_{\mathrm{J}}^{\mathrm{arr}}$. The JJ array thus implements a high-impedance transmission line characterized by its impedance $Z_{\mathrm{arr}} = \sqrt{L/C_g} < R_Q$ with the superconducting resistance quantum $R_Q \equiv h/(2e)^2 \simeq 6.5\ \mathrm{k}\Omega$. This transmission line is turned into a multimode microwave resonator by terminating it with impedance-unmatched loads at both ends. The left boundary (site $i = N + 1$) is connected to a 50 Ω measurement line and the right boundary (site $i = 0$) is galvanically coupled to a small Josephson junction ($E_{\mathrm{J}}/E_{\mathrm{c}} \sim 3$) acting as a nonlinear boundary condition. This small junction is characterized by its superconducting phase difference $\hat{\phi}_0$. The small $E_{\mathrm{J}}/E_{\mathrm{c}}$ ratio together with the large array impedance $Z_{\mathrm{arr}} \sim 0.1 R_Q$ triggers strong phase fluctuations $\langle \hat{\phi}_0^2 \rangle \simeq 1$ [9], making the terminal junction behave as an artificial atom.

Both the quantum impurity and the transmission line are made of SQUIDs, allowing us to fine-tune the frequency of the modes *in situ* by varying the current in an external coil. This allows us to reach the resonant condition $\omega_{\mathrm{in}} = 3\omega_{\mathrm{out}}$ favoring the generation of photon triplets at frequency ω_{out}. We designed the SQUIDs so that the loop area of the boundary SQUID with small E_{J} is much larger than that of the array SQUIDs [see Fig. 1(a)]. Then, a small variation of the external magnetic field significantly changes the flux Φ through the boundary SQUID, and thus its Josephson energy $E_{\mathrm{J}}(\Phi)$, without affecting much the flux Φ_{arr} through the array SQUIDs. The former tunes the mode frequencies

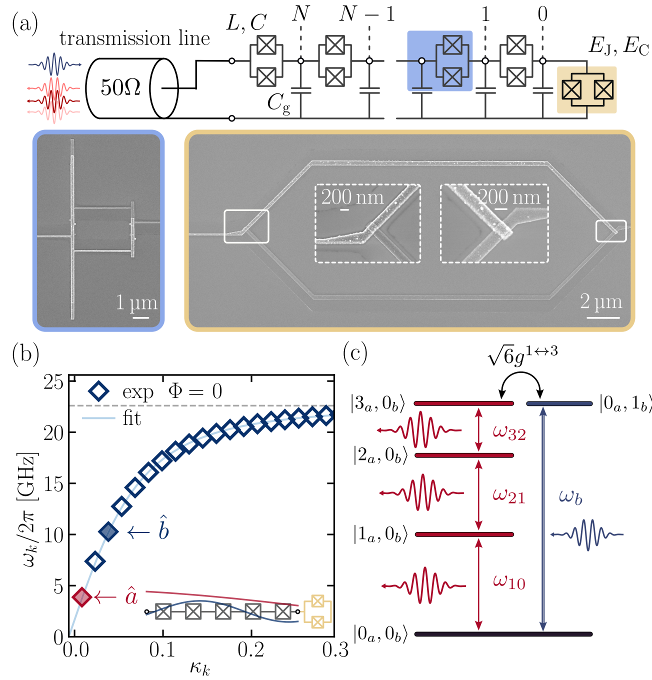

FIG. 1. (a) Schematics of the measured circuit. The SQUID array (blue) is characterized by its flux-tunable lumped element inductance L, capacitance C, and ground capacitance C_{g}. The chain contains $N = 200$ SQUIDs in the linear regime ($E_{\mathrm{J}}/E_{\mathrm{c}} = 284$ at zero flux) and is terminated by a nonlinear SQUID ($E_{\mathrm{J}}/E_{\mathrm{c}} \sim 3$ at zero flux), depicted in yellow and characterized by the flux-tunable Josephson energy $E_{\mathrm{J}}(\Phi)$ and capacitance C_{J}. SEM pictures: in the blue contour, image of a single SQUID of the array corresponding to the blue shaded area of panel (a); in the yellow contour, image of the nonlinear SQUID corresponding to the gold shaded area of panel (a). (b) Measured dispersion relation of the device showing the resonance frequencies ω_k of the first 19 modes as a function of their dimensionless wave vector κ_k ($0 < \kappa < \pi$). Relevant modes to the experiment are highlighted in red (mode $\hat{a}$) and blue (mode $\hat{b}$). The inset shows a sketch of their spatial profiles $\phi_{i,a}$ (red) and $\phi_{i,b}$ (blue) on sites $i = 0, \ldots, N$. The measured dispersion relation is fitted (plain blue line) to determine C_g (see Sec. A in [36]) Energy levels and transitions involved in the three-photon down-conversion fluorescence.

via the boundary condition, while the latter provides a slow change of the array plasma frequency (see Ref. [36]).

The Hamiltonian describing the circuit of Fig. 1 is

$$\hat{H} = \sum_k \hbar\omega_k \hat{a}_k^\dagger \hat{a}_k - E_J\left(\cos\hat{\phi}_0 - 1 + \hat{\phi}_0^2/2\right), \quad (1)$$

where $\hat{\phi}_0 = \sum_k \phi_{0,k}(\hat{a}_k^\dagger + \hat{a}_k)$, the coefficients $\phi_{0,k}$ correspond to the amplitude of mode k at the small junction, while $\hat{a}_k^\dagger$ and $\hat{a}_k$ are the normal mode creation and annihilation operators. Wave vectors κ_k, resonance frequencies ω_k, and spatial profiles $\phi_{i,k}$ of the normal modes are determined by solving the generalized eigenvalue problem of the linearized circuit. Figure 1(b) shows the measured frequency of the first 19 modes (out of 200) of the system as a function of their dimensionless wave vectors κ. The second term in Eq. (1) is the nonlinear part of the small junction cosine potential, $\cos\hat{\phi}_0 - 1 + \hat{\phi}_0^2/2 = \sum_{n>1}(-1)^n\hat{\phi}_0^{2n}/[(2n)!]$, the quadratic part already included in the normal mode decomposition.

This nonlinearity induces interactions between the array modes. Indeed, substituting $\hat{\phi}_0 = \sum_k \phi_{0,k}(\hat{a}_k^\dagger + \hat{a}_k)$ in the nonlinear term of the Hamiltonian, one readily obtains many terms of the form $\hat{a}_{k_n}^\dagger \cdots \hat{a}_{k_1}^\dagger \hat{a}_{l_m} \cdots \hat{a}_{l_1}$ that do not conserve the number of photons, but only its parity. In particular, the nonlinear part of Eq. (1) contains a term of the form $\hat{a}_{k_1}^\dagger \hat{a}_{k_2}^\dagger \hat{a}_{k_3}^\dagger \hat{a}_{k_4}$, corresponding to splitting a single photon in mode k_4 into three photons in modes k_1, k_2, and k_3. Flux tunability allows us to reach the resonance condition $\omega_{k=3} = 3\omega_{k=1}$, which selects the process $k_1 = k_2 = k_3 = 1$, and $k_4 = 3$ where a single photon of mode $k = 3$ is converted into three photons of mode $k = 1$. In the rest of the Letter, we denote the two relevant modes by operators $\hat{a}$ (low-frequency mode) and $\hat{b}$ (high-frequency mode). The explicit form of the corresponding conversion term in Eq. (1) is $\hat{H}_{ab} = \hbar g_{1\leftrightarrow 3}(\hat{a}^{\dagger 3}\hat{b} + \hat{b}^\dagger \hat{a}^3)$. If we take only the $\hat{\phi}_0^4$ term in the expansion of the cosine potential, the coupling strength is given by $\hbar g_{1\leftrightarrow 3} = (E_\mathrm{J}/6)\phi_{0,a}^3\phi_{0,b}$; higher-order terms can introduce corrections to this simple expression.

To achieve high conversion efficiency, it is essential to have strong phase zero-point fluctuations at the small junction site [see schematics in the inset of Fig. 1(b)]. This requirement is met thanks to the high impedance of the JJ array [38]. The second condition is that the single-photon state $|1_b\rangle$ of mode $\hat{b}$ and the three-photon state $|3_a\rangle$ of mode $\hat{a}$ are resonant [Fig. 1(c)]. The energy $E_{|3_a\rangle}$ of the latter state differs from $3\hbar\omega_a$ due to diagonal or self-Kerr terms of the nonlinear Hamiltonian. The flux tunability of the SQUIDs allows us to vary the detuning $E_{|3_a\rangle} - E_{|1_b\rangle}$. Large variations of the external magnetic field, which change the flux Φ in the small junction loop by multiples of Φ_0, leave the detuning unaffected, while changing significantly the flux Φ_arr through the array SQUIDs. Such a variation allows us to study various resonance conditions between $|1_b\rangle$ and $|3_a\rangle$, due to the modified array impedance, hence tuning different values of the resonance frequency.

Results—Prior to measuring the photon conversion process, we perform single-tone spectroscopy measurements to characterize our device and locate the external flux Φ leading to the multiphoton resonance condition. The sample is cooled down to a temperature $T \sim 12$ mK inside a dilution refrigerator. The reflection coefficient $S_{11}(\omega_\mathrm{d}) = a_\mathrm{out}(\omega_\mathrm{d})/a_\mathrm{in}(\omega_\mathrm{d})$ is recorded using a vector network analyzer, where $a_\mathrm{in}(\omega_\mathrm{d})$ and $a_\mathrm{out}(\omega_\mathrm{d})$ are, respectively, the input and output fields at the drive frequency ω_d.

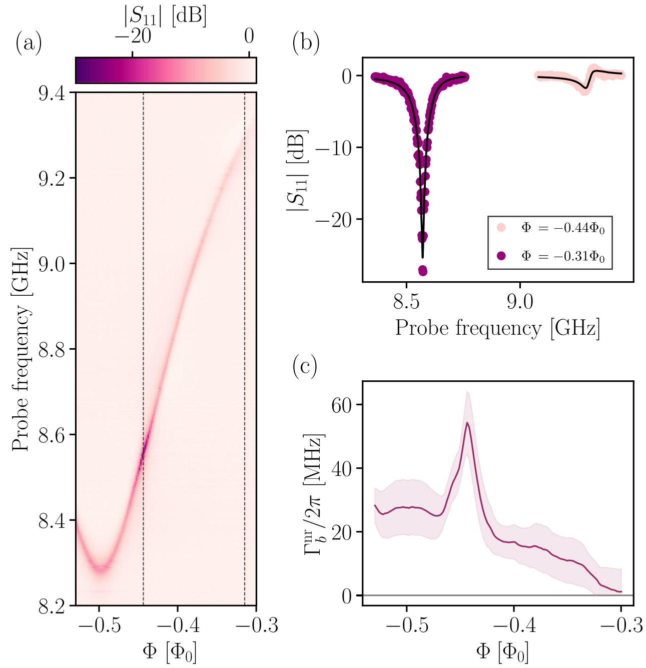

FIG. 2. (a) Color map of the measured magnitude of the reflection coefficient $|S_{11}(\omega_\mathrm{d})|$ of mode $\hat{b}$ versus drive frequency ω_d and external magnetic flux Φ threading the small JJ loop. The mode frequency ω_b changes due to the flux dependence of the Josephson energy of the small JJ loop. A significant drop in S_{11} around $\omega_b/2\pi = 8.6$ GHz and $\Phi = -0.44\Phi_0$ signals an enhancement of photon loss when $\omega_b \simeq 3\omega_a$. Note that the fluorescence measurement was in fact carried out at a different arch. The corresponding data show a spurious mode that does not affect the analysis. They are available in Fig. S1 [36]. (b) Slices corresponding to the vertical dashed lines of panel (a) showing a drastic attenuation of the reflected signal close to $\Phi = -0.44\Phi_0$ attributed to photon down-conversion processes. (c) Nonradiative losses $\Gamma_b^\mathrm{nr}/2\pi$ of mode $\hat{b}$ as a function of Φ extracted by fitting $S_{11}(\omega_\mathrm{d})$ to Eq. (2). Imperfect isolation of the microwave components used in the experiment [39] leads to the asymmetric lineshape on panel (b), not described by Eq. (2). The shaded area around the data shows the resulting uncertainty in the extracted nonradiative losses when taking into account these imperfections.

Figure 2(a) shows a map of the magnitude of the reflection coefficient $|S_{11}(\omega)|$ measured in a frequency window close to mode b resonance frequency and for varying Φ. From this measurement, we clearly see that $|S_{11}(\omega)|$ almost vanishes around $\Phi = -0.44\Phi_0$. Figure 2(b) shows constant flux cuts of $|S_{11}(\omega)|$ through the minimal value (purple) and far away from this minimum (pink). A drastic -20 dB attenuation of the reflected signal is observed. This decrease in the reflected signal amplitude implies an increase in losses of ω_b photons, that we attribute to the photon conversion process.

In order to extract mode b frequency and decay rates, we fit the measured reflection coefficient to the following expression valid in the vicinity of mode $\hat{b}$ resonant frequency:

$$S_{11}(\omega_\mathrm{d}) = \frac{\Gamma_b - 2\Gamma_b^\mathrm{r} + 2i(\omega_b - \omega_\mathrm{d})}{\Gamma_b - 2i(\omega_b - \omega_\mathrm{d})}, \qquad (2)$$

where Γ_b is the total photon decay rate in mode b, while Γ_b^r is the radiative decay rate due to coupling to the measurement line. Figure 2(c) shows the fitted values of nonradiative decay rate $\Gamma_b^\mathrm{nr} \equiv \Gamma_b - \Gamma_b^\mathrm{r}$ as a function of the external flux Φ. From this measurement, we clearly see a sharp increase in the internal losses of mode b, going from a baseline $\Gamma_b^{\mathrm{nr},0} \simeq 2\pi \times 20$ MHz to $\Gamma_b^\mathrm{nr} = \Gamma_b^{\mathrm{nr},0} + \Gamma^{1\leftrightarrow 3} = 2\pi \times 60$ MHz on resonance. We repeated the experiment at other values of the external flux, leading to lower array impedances, and to a resonance condition $\omega_a \simeq 3\omega_b$ occurring at different frequencies. At the lowest impedance, we found a sevenfold increase of Γ_b^nr. Thus, the observed loss enhancement is not due to a spurious resonance which would be expected to have a fixed frequency (see Sec. B in [36]). At this flux bias point, the three-photon conversion losses overcome other nonradiative losses, namely $\Gamma^{1\leftrightarrow 3} > \Gamma_b^{\mathrm{nr},0}$. Such inelastic effects induced by a boundary were already reported [10,11]. We will demonstrate now that their microscopic origin is indeed photon down-conversion.

Our measurement starts by setting the external flux to the value Φ^opt corresponding to the peak in the inelastic losses Γ_b^nr [Fig. 2(b)]. The system is then continuously driven at frequency $\omega_b/2\pi = 9.13$ GHz. Anticipating triplet emission, the spectra are acquired on a 1 GHz span around $\omega_a/2\pi \simeq 3.16$ GHz with a resolution bandwidth of 5 MHz using a power spectrum analyzer, with a sweep time of 1 s. To circumvent low frequency drifts that would completely blur the measurement, the spectrum is alternatively measured with driving tone and without driving tone [Fig. 3(a)]. Each on-off sequence is repeated 22 500 times. Figure 3(b) shows the spectrum measured with (dark red curve) and without (light red curve) a traveling wave parametric amplifier (TWPA) [40] for otherwise identical experimental parameters including the measurement time. Given the time of about 20 h required to obtain a signal with very low signal to noise ratio (SNR) using only a low-noise amplifier as the first stage of amplification, this measurement clearly demonstrates the advantages of using a TWPA in such a low-power microwave quantum optics experiment. More specifically, the TWPA can improve the SNR up to 14 dB. Interestingly, this improved SNR allows us to resolve the asymmetric shape of the fluorescence peak, which can be attributed to the anharmonicity of mode $\hat{a}$ as will be discussed later. We have checked that the fluorescence signal at $\omega_a \simeq \omega_b/3$ quickly disappears when detuning the pump from frequency ω_b, showing that the low frequency photons are indeed coming from down-conversion. Another important feature of the fluorescence signal is its dependence on the drive power P_in. We measured several emission spectra for different values of P_in, while still remaining in the single-photon regime. The resulting spectra are shown in Fig. 3(c). The output power increases linearly with input power P_in, as expected for a spontaneous down-conversion process (see Sec. C in [36]).

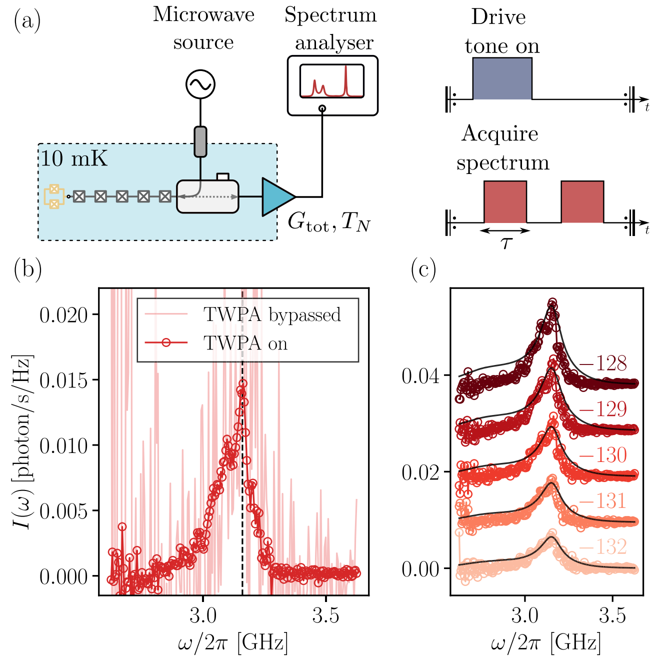

FIG. 3. Spectrum of the emitted down-converted photons. (a) Left panel: a simplified schematic of the measurement setup. Right panel: on-off measurement scheme. (b) Emission spectrum at a fixed drive frequency $\omega_\mathrm{d} = \omega_b = 2\pi \times 9.13$ GHz with (dark red) and without (light red) TWPA for a drive power $P_\mathrm{in} = -129$ dBm. (c) Emission spectra for increasing driving tone power P_in (from light red to dark red, vertically shifted by 0.01 for clarity). The values of P_in are given in dBm by the colored negative numbers. Black solid lines show the emission spectra calculated theoretically. All shown data were acquired at $\Phi = -0.44\Phi_0$.

Theoretical model—To understand the asymmetric spectral shape of the measured fluorescence signal, we calculate it theoretically using the quantum regression theorem for a multilevel system coupled to a radiation field [41]. (See Sec. D of [36] for more detail.) Focusing on the weak drive limit, we truncate the system Hilbert space to the five levels shown in Fig. 1(c): $|0_a 0_b\rangle, |0_a 1_b\rangle, |3_a 0_b\rangle, |2_a 0_b\rangle, |1_a 0_b\rangle$ with energies $0, \hbar\omega_b, \hbar(\omega_{32} + \omega_{21} + \omega_{10}), \hbar(\omega_{21} + \omega_{10}), \hbar\omega_{10}$, respectively. Strictly speaking, ω_{10} and ω_b are different from the harmonic frequencies ω_k in Eq. (1) due to nonlinear corrections; however, they are determined experimentally by the reflection measurement ($2\pi \times 3.16$ GHz and $2\pi \times 9.13$ GHz, respectively), which also gives the modes' radiative ($\Gamma_a^\mathrm{r} = 2\pi \times 84$ MHz, $\Gamma_b^\mathrm{r} = 2\pi \times 53$ MHz) and nonradiative ($\Gamma_a^\mathrm{nr} = 2\pi \times 57$ MHz and $\Gamma_b^\mathrm{nr} = 2\pi \times 22$ MHz) decay rates.

The remaining parameters of the model are the higher transition frequencies ω_{32}, ω_{21} and the coupling $g_{1\leftrightarrow 3}$. In principle, they could be found from the $\hat{\phi}_0^4$ term of the cosine potential. Then, neglecting pure dephasing, we find the fluorescence spectrum consisting of three broadened peaks centered at ω_{10}, ω_{21}, and $\omega_d - \omega_{10} - \omega_{21}$ (indeed, if ω_d is detuned from $\omega_{32} + \omega_{21} + \omega_{10}$, the state $|3_a 0_b\rangle$ is only virtually populated due to energy conservation, so there is no emission at frequency ω_{32}). This shape does not fully agree with the experiment, which leads us to conclude that $\hat{\phi}_0^4$ expansion of the cosine potential is not sufficient. Higher-order terms can produce rather complex nonlinear effects already at a few-photon level [42,43], whose study is beyond the scope of the present Letter. So, we constrain $\omega_{32} + \omega_{21} + \omega_{10} = \omega_b$ (since the spectra were obtained at the flux corresponding to maximum conversion) and use ω_{21} and $g_{1\leftrightarrow 3}$ as global fitting parameters (the same values for each input power P_{in}). The resulting values $\omega_{21} \approx 2\pi \times 2.7$ GHz and $g_{1\leftrightarrow 3} \approx 2\pi \times 7$ MHz give the theoretical curves in Fig. 3(c). (See Sec. F of [36].) Here, we have attributed all nonradiative losses to decay into an unmonitored reservoir, which allows us to obtain a relatively compact theoretical expression for the spectral density of down-converted photons. (See Sec. D of [36].) We also investigated nonradiative broadening by pure dephasing in Secs. E and F in [36]. Overall, the emission spectrum can have a complicated structure, determined by several unknowns. We decided to keep this number of fitting parameters as low a possible. Despite this, our model gives a reasonable account of the effect of drive frequency detuning and variation of input power.

Conclusion and outlook—We have observed three-photon down-conversion fluorescence for a quantum impurity simulator in circuit QED. This nonparametric process results in the spontaneous decay of a single photon into three photons of lower energy. First, a microwave reflection experiment revealed a strong resonantlike depletion of the drive tone suggesting the presence of an additional loss channel related to the resonant photon conversion process. Second, using state-of-the-art near-quantum-limited parametric amplification, we could directly measure the down-converted photons, which constitutes, to the best of our knowledge, the first model-independent detection of a predicted ultrastrong coupling effect [29,30]. This fluorescence spectrum is well reproduced by an effective few-level model. Our finding shows that microwave quantum optics techniques can shed new light on the physics of strongly interacting quantum impurities.

Our results also have implications for the fast-growing field of high-impedance superconducting quantum bits, which promise very long coherence times [44,45]. The nonlinear couplings we have highlighted here form a non-negligible loss channel that could limit the coherence of these circuits, and understanding their potential impact will probably require models that go beyond the initial studies on this subject [46–48]. This extremely efficient frequency conversion process could be an interesting alternative for generating Schrödinger cat states with an arbitrary number of components [49]. Further investigation of the spontaneous down-conversion process could also involve the study of correlations between the emitted photons [50]. In addition, the future observation of the theoretically predicted [17–19,22,23,51] broadband and universal inelastic down-conversion for long Josephson arrays involving many modes remains another important challenge for superconducting quantum simulators.

Acknowledgments—This work was supported by the QuantERA grant SiUCs (Grant No. 731473). The sample was fabricated in the clean room facility of Institute Neel, Grenoble. We sincerely thank all the clean room staff for help with fabrication of the devices. We would like to acknowledge E. Eyraud for his extensive help in the installation and maintenance of the cryogenic setup. We also thank J. Jarreau, D. Dufeu, and L. Del Rey for their support with the experimental equipment. We are grateful to J. Ankerhold, M. Resch, and R. Albert for insightful discussions regarding this project and to Q. Ficheux and P. Forn-Diaz for their critical reading of the manuscript. We thank the members of the superconducting circuits group at Neel Institute for helpful discussions.

[1] A. Blais, A. L. Grimsmo, S. M. Girvin, and A. Wallraff, Rev. Mod. Phys. **93**, 025005 (2021).

[2] A. A. Houck, H. E. Türeci, and J. Koch, Nat. Phys. **8**, 292 (2012).

[3] I. Carusotto, A. A. Houck, A. J. Kollár, P. Roushan, D. I. Schuster, and J. Simon, Nat. Phys. **16**, 268 (2020).

[4] D. Meiser and P. Meystre, Phys. Rev. A **74**, 065801 (2006).

[5] N. M. Sundaresan, Y. Liu, D. Sadri, L. J. Szocs, D. L. Underwood, M. Malekakhlagh, H. E. Türeci, and A. A. Houck, Phys. Rev. X **5**, 021035 (2015).

[6] J. P. Martinez, S. Leger, N. Gheeraert, R. Dassonneville, L. Planat, F. Foroughi, Y. Krupko, O. Buisson, C. Naud, W. Hasch-Guichard, S. Florens, I. Snyman, and N. Roch, npj Quantum Inf. **5**, 1829 (2019).

[7] R. Kuzmin, N. Mehta, N. Grabon, R. Mencia, and V. E. Manucharyan, npj Quantum Inf. **5**, 20 (2019).

[8] P. Forn-Diaz, J. J. Garcia-Ripoll, B. Peropadre, J.-L. Orgiazzi, M. A. Yurtalan, R. Belyansky, C. M. Wilson, and A. Lupascu, Nat. Phys. **13**, 39 (2017).

[9] S. Léger, J. Puertas-Martínez, K. Bharadwaj, R. Dassonneville, J. Delaforce, F. Foroughi, V. Milchakov, L. Planat, O. Buisson, C. Naud, W. Hasch-Guichard, S. Florens, I. Snyman, and N. Roch, Nat. Commun. **10**, 5259 (2019).

[10] R. Kuzmin, N. Grabon, N. Mehta, A. Burshtein, M. Goldstein, M. Houzet, L. I. Glazman, and V. E. Manucharyan, Phys. Rev. Lett. **126**, 197701 (2021).

[11] S. Léger, T. Sépulcre, D. Fraudet, O. Buisson, C. Naud, W. Hasch-Guichard, S. Florens, I. Snyman, D. M. Basko, and N. Roch, SciPost Phys. **14**, 130 (2023).

[12] N. Mehta, R. Kuzmin, C. Ciuti, and V. E. Manucharyan, Nature (London) **613**, 650 (2023).

[13] A. Roy, D. Schuricht, J. Hauschild, F. Pollmann, and H. Saleur, Nucl. Phys. **B968**, 115445 (2021).

[14] A. Roy and S. L. Lukyanov, Nat. Commun. **14**, 7433 (2023).

[15] G. Schön and A. D. Zaikin, Phys. Rep. **198**, 237 (1990).

[16] K. Le Hur, Phys. Rev. B **85**, 140506(R) (2012).

[17] M. Goldstein, M. H. Devoret, M. Houzet, and L. I. Glazman, Phys. Rev. Lett. **110**, 017002 (2013).

[18] E. Sanchez-Burillo, D. Zueco, J. J. Garcia-Ripoll, and L. Martin-Moreno, Phys. Rev. Lett. **113**, 263604 (2014).

[19] N. Gheeraert, X. H. H. Zhang, T. Sépulcre, S. Bera, N. Roch, H. U. Baranger, and S. Florens, Phys. Rev. A **98**, 043816 (2018).

[20] M. Houzet and L. I. Glazman, Phys. Rev. Lett. **125**, 267701 (2020).

[21] A. Burshtein, R. Kuzmin, V. E. Manucharyan, and M. Goldstein, Phys. Rev. Lett. **126**, 137701 (2021).

[22] A. Burshtein and M. Goldstein, PRX Quantum **5**, 020323 (2024).

[23] M. Houzet, T. Yamamoto, and L. I. Glazman, Phys. Rev. B **109**, 155431 (2024).

[24] S.-P. Wang, A. Mercurio, A. Ridolfo, Y. Wang, M. Chen, T. Li, F. Nori, S. Savasta, and J. Q. You, arXiv:2401.02738.

[25] N. Mehta, C. Ciuti, R. Kuzmin, and V. E. Manucharyan, arXiv:2210.14681.

[26] A. O. Caldeira and A. J. Leggett, Ann. Phys. (N.Y.) **149**, 374 (1983).

[27] K. Bencheikh, F. Gravier, J. Douady, A. Levenson, and B. Boulanger, C.R. Phys. **8**, 206 (2007).

[28] A. Vrajitoarea, R. Belyansky, R. Lundgren, S. Whitsitt, A. V. Gorshkov, and A. A. Houck, arXiv:2209.14972.

[29] A. F. Kockum, V. Macri, L. Garziano, S. Savasta, and F. Nori, Sci. Rep. **7**, 5313 (2017).

[30] K. Koshino, T. Shitara, Z. Ao, and K. Semba, Phys. Rev. Res. **4**, 013013 (2022).

[31] L. Magazzu, P. Forn-Díaz, R. Belyansky, J. L. Orgiazzi, M. A. Yurtalan, M. R. Otto, A. Lupaşcu, C. M. Wilson, and M. Grifoni, Nat. Commun. **9**, 1403 (2018).

[32] E. Zakka-Bajjani, F. Nguyen, M. Lee, L. R. Vale, R. W. Simmonds, and J. Aumentado, Nat. Phys. **7**, 599 (2011).

[33] I.-M. Svensson, A. Bengtsson, J. Bylander, V. Shumeiko, and P. Delsing, Appl. Phys. Lett. **113**, 022602 (2018).

[34] C. W. S. Chang, C. Sabin, P. Forn-Díaz, F. Quijandría, A. M. Vadiraj, I. Nsanzineza, G. Johansson, and C. M. Wilson, Phys. Rev. X **10**, 011011 (2020).

[35] S. Gasparinetti, M. Pechal, J.-C. Besse, M. Mondal, C. Eichler, and A. Wallraff, Phys. Rev. Lett. **119**, 140504 (2017).

[36] See Supplemental Material at http://link.aps.org/supplemental/10.1103/PhysRevLett.134.013804, which includes Ref. [37], for details on the fit of the dispersion relation, on losses at different values of the chain impedance, on the power dependence of the fluorescence, on theoretical calculations of the fluorescence spectrum with and without pure dephasing, and on the comparison between theory and experiment.

[37] T. Weißl, B. Küng, E. Dumur, A. K. Feofanov, I. Matei, C. Naud, O. Buisson, F. W. J. Hekking, and W. Guichard, Phys. Rev. B **92**, 104508 (2015).

[38] U. Vool and M. Devoret, Int. J. Circuit Theory Appl. **45**, 897 (2017).

[39] D. Rieger, S. Günzler, M. Spiecker, A. Nambisan, W. Wernsdorfer, and I. M. Pop, Phys. Rev. Appl. **20**, 014059 (2023).

[40] A. Ranadive, M. Esposito, L. Planat, E. Bonet, C. Naud, O. Buisson, W. Guichard, and N. Roch, Nat. Commun. **13**, 1737 (2022).

[41] B. R. Mollow, Phys. Rev. **188**, 1969 (1969).

[42] A. M. Hriscu and Y. V. Nazarov, Phys. Rev. Lett. **106**, 077004 (2011).

[43] W. C. Smith, A. Borgognoni, M. Villiers, E. Roverc'h, J. Palomo, M. R. Delbecq, T. Kontos, P. Campagne-Ibarcq, B. Douçot, and Z. Leghtas, arXiv:2312.15075.

[44] A. Somoroff, Q. Ficheux, R. A. Mencia, H. Xiong, R. Kuzmin, and V. E. Manucharyan, Phys. Rev. Lett. **130**, 267001 (2023).

[45] A. Gyenis, P. S. Mundada, A. Di Paolo, T. M. Hazard, X. You, D. I. Schuster, J. Koch, A. Blais, and A. A. Houck, PRX Quantum **2**, 010339 (2021).

[46] A. Mizel and Y. Yanay, Phys. Rev. B **102**, 014512 (2020).

[47] A. Di Paolo, T. E. Baker, A. Foley, D. Sénéchal, and A. Blais, npj Quantum Inf. **7**, 11 (2021).

[48] K. Kaur, T. Sépulcre, N. Roch, I. Snyman, S. Florens, and S. Bera, Phys. Rev. Lett. **127**, 237702 (2021).

[49] A. Marquet, A. Essig, J. Cohen, N. Cottet, A. Murani, E. Abertinale, S. Dupouy, A. Bienfait, T. Peronnin, S. Jezouin, R. Lescanne, and B. Huard, Phys. Rev. X **14**, 021019 (2024).

[50] M. D. Silva, D. Bozyigit, A. Wallraff, and A. Blais, Phys. Rev. A **82**, 043804 (2010).

[51] B. Peropadre, D. Zueco, D. Porras, and J. J. Garcia-Ripoll, Phys. Rev. Lett. **111**, 243602 (2013).